

Launching of jets by cold, magnetized disks in Kerr Metric

Aleksander Sądowski¹ and Marek Sikora¹

N. Copernicus Astronomical Center, Polish Academy of Sciences, Bartycka 18, 00-716 Warszawa, Poland
e-mail: as@camk.edu.pl e-mail: sikora@camk.edu.pl

Received ????; accepted ????

ABSTRACT

We confirm discovery by Cao that in the vicinity of fast rotating black holes jets can be launched centrifugally by cold, magnetized disks even for nearly vertically shaped magnetic flux surfaces. Outflows produced under such extreme conditions are investigated via studying kinematics of test particles in the force-free magnetosphere approximation. Implications of a possibility of magneto-centrifugal launching of very well collimated central outflows around the fast rotating black holes are discussed in the general context of the jet formation scenarios in AGNs.

Key words. black hole physics – accretion disks – magnetic fields

1. Introduction

According to a popular class of astrophysical jet models they are powered by rotational energy of accretion disks and mass loaded via ‘magnetocentrifugal’ forces. For Newtonian accretion disks such models require the poloidal magnetic field lines to be inclined to the geometrically thin accretion disk by less than 60 degrees, independently on a distance from the central object (Blandford & Payne 1982). For disks around black holes (BHs) this angle depends on the radius and the BH spin (Cao 1997; Lyutikov 2009). It is the larger the smaller is the distance and the larger is the BH spin. At the inner edge of a Keplerian disk (located at the marginally stable orbit - r_{ms}) and for the maximal BH spin it approaches 90°. We confirm these results and investigate the kinematics of test particles in the fixed force-free magnetosphere. Our paper is organized as follows. General equations describing the particle kinematics are derived in §2. Geometry of the effective equipotential surfaces and of ‘light cylinders’ are presented in §3. Kinematics of test particles and its dependence on the BH spin and the launching distance is illustrated in §4. Results are discussed in a general context of production of relativistic jets in active galactic nuclei in §5 and summarised in §6.

2. A rigid rotation of particle trajectories in the Kerr metric

Kinematics of particles forced by magnetic fields to move on rigidly rotating trajectories is convenient to investigate in a frame co-rotating with magnetic field lines. In such a frame the norm of a 4-velocity, $u_i u^i = -1$, is in the Kerr metric given by equation:

$$(g_{tt} + 2g_{t\phi}\Omega_0 + g_{\phi\phi}\Omega_0^2)(u^t)^2 + 2(g_{t\phi} + g_{\phi\phi}\Omega_0)u^t u^{\phi'} + g_{\phi\phi}(u^{\phi'})^2 + g_{rr}(u^r)^2 + g_{\theta\theta}(u^\theta)^2 = -1, \quad (1)$$

where $\phi' = \phi - \Omega_0 t$, $u^{\phi'} = u^\phi - \Omega_0 u^t$, $\Omega_0 = \text{const}$, the t , ϕ , r , and θ are the Boyer-Lindquist coordinates, and $g_{ik} =$

$g_{ik}(r, \theta; a)$ are the Kerr metric components. Through the paper the following quantities are expressed in dimensionless units: radius $r : r/(GM/c^2)$, BH spin $a^* = J/(GM^2/c)$, and angular velocity $\Omega_0 : \Omega_0/(c^3/GM)$, where M and J are the BH mass and angular momentum, respectively.

For a particle trajectory which in the rotating frame is described by functions $r = r(\theta)$ and $\phi' = \phi'(\theta)$, the r and ϕ' components of the particle 4-velocity are $u^r = r_{,\theta} u^\theta$ and $u^{\phi'} = \phi'_{,\theta} u^\theta$, respectively. Then the norm of the 4-velocity reads

$$\tilde{g}_{tt}(u^t)^2 + 2\tilde{g}_{t\theta}u^t u^\theta + \tilde{g}_{\theta\theta}(u^\theta)^2 = -1, \quad (2)$$

where

$$\tilde{g}_{tt} = g_{tt} + 2g_{t\phi}\Omega_0 + g_{\phi\phi}\Omega_0^2, \quad (3)$$

$$\tilde{g}_{t\theta} = (g_{t\phi} + g_{\phi\phi}\Omega_0)\phi'_{,\theta}, \quad (4)$$

$$\tilde{g}_{\theta\theta} = g_{\theta\theta} + g_{rr}(r_{,\theta})^2 + g_{\phi\phi}(\phi'_{,\theta})^2. \quad (5)$$

Noting that

$$\tilde{u}_t = \tilde{g}_{tt}u^t + \tilde{g}_{t\theta}u^\theta = -\tilde{\epsilon}, \quad (6)$$

where $\tilde{\epsilon}$ is the constant of motion of particle moving along a rigidly rotating trajectory, one can find inserting u_t from Eq. (6) into Eq. (2) that

$$u^\theta = \sqrt{\frac{(\tilde{\epsilon})^2 - (-\tilde{g}_{tt})}{(-\tilde{g}_{tt})\tilde{g}_{\theta\theta} + (\tilde{g}_{t\theta})^2}}, \quad (7)$$

and

$$u^t = \frac{\tilde{\epsilon}}{(-\tilde{g}_{tt})} + \frac{\tilde{g}_{t\theta}}{(-\tilde{g}_{tt})} u^\theta = \frac{\tilde{\epsilon}}{(-\tilde{g}_{tt})} + \frac{\tilde{g}_{t\theta}}{(-\tilde{g}_{tt})} \sqrt{\frac{(\tilde{\epsilon})^2 - (-\tilde{g}_{tt})}{(-\tilde{g}_{tt})\tilde{g}_{\theta\theta} + (\tilde{g}_{t\theta})^2}}. \quad (8)$$

Hence, for a fixed particle trajectory and a given constant of motion $\tilde{\epsilon}$ kinematics of a test particle is fully determined. This kinematics can be illustrated in the locally

non-rotating frame (Bardeen, Press, & Teukolsky 1972), i.e. the frame of zero-angular-momentum-observers (ZAMO). In such a frame the line element is

$$ds^2 = (g_{tt} + \omega g_{t\phi}) dt^2 + g_{\phi\phi} (d\phi - \omega dt)^2 + g_{rr} dr^2 + g_{\theta\theta} d\theta^2, \quad (9)$$

where $\omega = -g_{t\phi}/g_{\phi\phi}$ is the angular velocity of 'the dragged inertial frames'. Then the projection of the 4-velocity onto the orthonormal tetrad of the local Minkowski space can be used to calculate the Lorentz factor and velocity components of a particle in the ZAMO frame:

$$\gamma = u^{(t)} = u^t \sqrt{-g_{tt} + g_{t\phi}^2/g_{\phi\phi}}, \quad (10)$$

$$v^{(\phi)} = \frac{u^{(\phi)}}{u^{(t)}} = \left(\frac{\phi',_{\theta} u^{\theta}}{u^t} + (\Omega_0 - \omega) \right) \sqrt{\frac{g_{\phi\phi}}{-g_{tt} + g_{t\phi}^2/g_{\phi\phi}}}, \quad (11)$$

$$v^{(p)} \equiv \sqrt{v^{(r)^2} + v^{(\theta)^2}} = \frac{u^{\theta}}{u^t} \sqrt{\frac{g_{rr} r_{,\theta} + g_{\theta\theta}}{-g_{tt} + g_{t\phi}^2/g_{\phi\phi}}}. \quad (12)$$

where the physical velocities $v^{(i)}$ are expressed in the speed of light units.

3. Effective potential

An effective potential defined as the minimum energy of test particles forced to rotate with a given angular velocity Ω_0 is $V_{eff} = \sqrt{-\tilde{g}_{tt}}$ (obtained from Eq. (7) setting $u^{\theta} = 0$). Its equipotential surfaces, $V_{eff}(r, \theta) = \text{const}$, are illustrated in Fig. 1. They are enclosed between the inner and outer 'light cylinders' given by $\tilde{g}_{tt} = 0$ (Lyutikov 2009). Locations of the inner and outer light cylinders in the equatorial plane are presented in Fig. 2. For a given spin the cylinders coincide at the photon orbit. For $a^* > 0.91$ and the angular velocity Ω_0 corresponding to the marginally stable orbit r_{ms} the outer light cylinder is enclosed by the BH ergosphere. In Fig. 3 we show the dependence of the equatorial and asymptotic locations of the outer light cylinder on the BH spin for Ω_0 calculated at the marginally stable orbit. The asymptotic radius is always close to its equatorial plane value (e.g. $14.7M$ vs $13.6M$ for a non-rotating BH).

Equipotential surfaces, $dV_{eff} = 0$, intersect the equatorial plane at angles

$$\tan \xi = -r \left(\frac{d\theta}{dr} \right)_{\theta=\pi/2} = r \left(\frac{V_{eff,r}}{V_{eff,\theta}} \right)_{\theta=\pi/2}. \quad (13)$$

Since $V_{eff,\theta}|_{\theta=\pi/2} = 0$, while $V_{eff,r}|_{\theta=\pi/2} = 0$ only at $r = r_0$ at which the Keplerian law is satisfied, i.e.

$$\Omega_0 = \frac{1}{r_0^{3/2} + a}. \quad (14)$$

this angle is $\xi = \pi/2$ for all radii but $r = r_0$. At $r = r_0$ this angle can be found by applying in Eq. (13) the L'Hospital's rule and by noting that $V_{eff,r\theta}|_{\theta=\pi/2} = 0$. This gives

$$\begin{aligned} \tan \xi_0 &= r_0 \sqrt{-\left(\frac{V_{eff,rr}}{V_{eff,\theta\theta}} \right)_{\theta=\pi/2, r=r_0}} = \\ &= \sqrt{\frac{3}{1 - 4ar_0^{-3/2} + 3a^2 r_0^{-2}}}. \end{aligned} \quad (15)$$

This formula fully agrees with the formula obtained by Cao (1997) and Lyutikov (2009). Dependence of ξ_0 on the radius r_0 and on the BH spin is shown in Fig. 4.

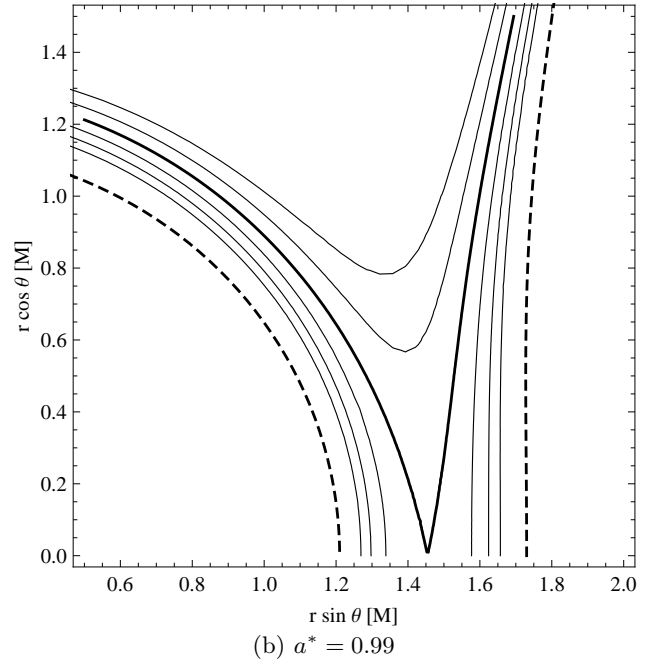
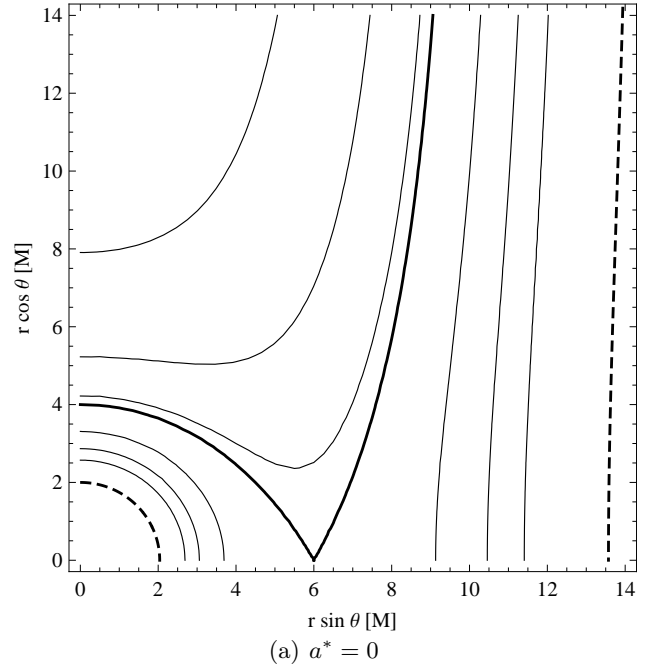


Fig. 1. Equipotential surfaces of the effective potential ($V_{eff} = \sqrt{-\tilde{g}_{tt}}$) for $\Omega_0 = \Omega_0(r = r_{ms}, a^*)$ for a non-rotating (top) and spinning (bottom panel) BHs. The thick solid lines represent $V_{eff}(r, \theta) = V_0 \equiv V_{eff}(r = r_{ms}, \theta = \pi/2)$ being the effective potential crossing the equator at $r = r_{ms}$. The dashed lines present locations of the inner and outer light cylinders. The thin solid lines are drawn for the following values of the effective potential: $\frac{6}{9}, \frac{7}{9}, \frac{8}{9}, \frac{10}{9}, \frac{11}{9} V_0$.

4. Kinematics of test particles in a force-free magnetosphere

4.1. Purely poloidal magnetic fields

For a strong dynamical domination of large scale magnetic fields driven by an accretion disk, test particles are re-

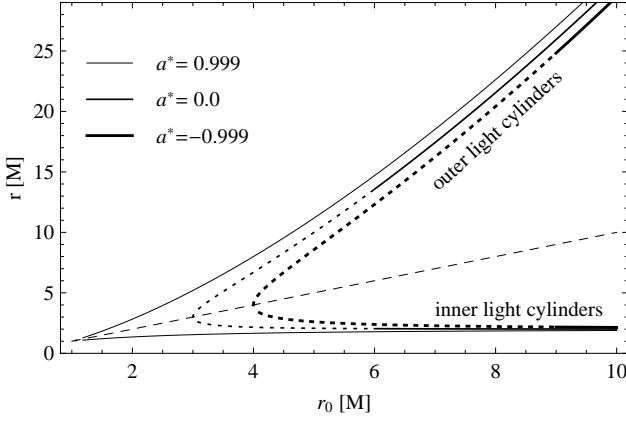


Fig. 2. Locations of the inner and outer light cylinders for $\theta = \pi/2$ as a function of radius r_0 defining the angular velocity Ω_0 . Inner and outer cylinders are represented by curves below and above the dashed line $r = r_0$, respectively. Dotted curves denote locations of light cylinders for $r_0 < r_{ms}$. Profiles for three values of BH spin: $-0.999, 0, 0.999$ are presented.

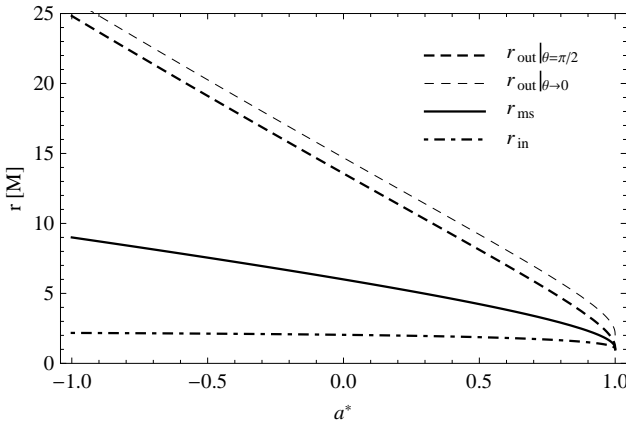


Fig. 3. Locations of the light cylinders for $\Omega_0 = \Omega_0(r = r_{ms})$ versus BH spin. Location of the outer light cylinder is shown for the equatorial plane (thick, dashed line) as well as its asymptotic ($\theta \rightarrow 0$) value (thin, dashed line).

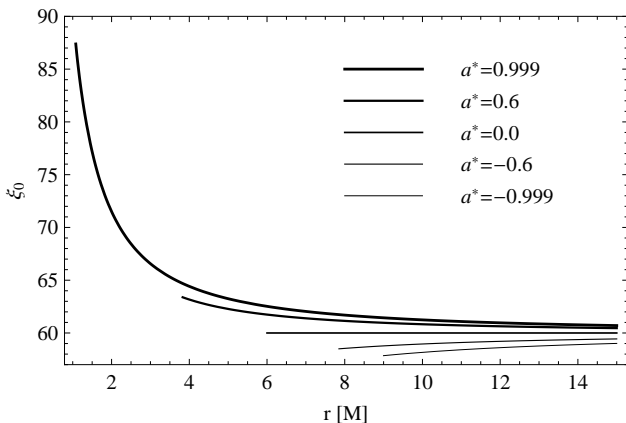


Fig. 4. The critical angle ξ_0 dependence on the radius r_0 . Profiles for different BH spins, starting at the marginally stable orbits, are shown.

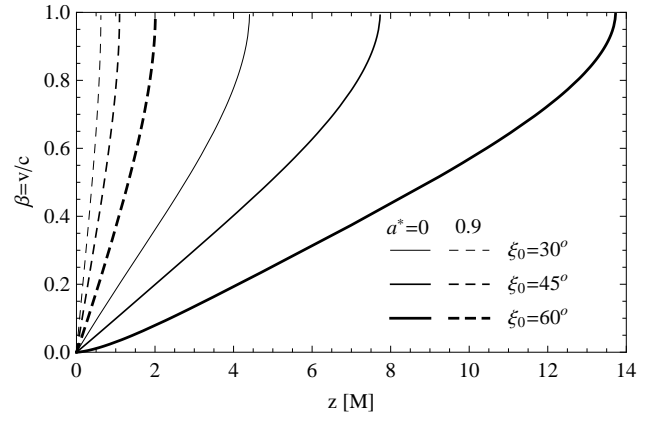


Fig. 5. Dynamics of a particle moving along a purely poloidal magnetic field lines anchored at r_{ms} and inclined at different angles for non-spinning (solid) and spinning (dashed lines) BHs. The horizontal axis represents the vertical coordinate z .

stricted to move along magnetic field lines. Being anchored to a differentially rotating accretion disk, the poloidal magnetic field generates differentially rotating magnetosphere. Trajectories of test particles can then be identified with magnetic field lines rotating with an angular velocity of their foot-points (Ferraro 1937). For purely poloidal magnetic fields such trajectories are in the co-rotating frame planar ($\phi' = \text{const}$), the metric component $\tilde{g}_{t\theta} = 0$ and equations (7) and (8) reduce to

$$u^\theta = \sqrt{\frac{(\tilde{\epsilon}_0)^2 - (-\tilde{g}_{tt})}{(-\tilde{g}_{tt})\tilde{g}_{\theta\theta}}}, \quad (16)$$

$$u^t = \frac{\tilde{\epsilon}_0}{(-\tilde{g}_{tt})}, \quad (17)$$

where $\tilde{\epsilon}_0^2 = -\tilde{g}_{tt}(\theta = \pi/2, r = r_0)$, $\tilde{g}_{ik} = \tilde{g}_{ik}(\theta, r(\theta; r_0))$, and $r(\theta; r_0)$ is the shape of the magnetic field surface which is determined by the shape of poloidal magnetic field lines.

Test particles can be pulled from the cold disk by centrifugal forces provided the inclination of magnetic field surfaces at the foot-point is smaller than ξ_0 and they can proceed further provided the shape of poloidal magnetic field lines is such that along them the condition $-\tilde{g}_{tt} < \tilde{\epsilon}_0^2$ is satisfied.

Examples of kinematics of the test particles are plotted in Fig. 4. The illustrated cases are calculated for magnetic field lines anchored at the marginally stable orbit and having shape

$$r = r_0 \frac{\tan \xi_0}{(\sin \theta \tan \xi - \cos \theta)}, \quad (18)$$

which in the coordinate plane $(r \cos \theta, r \sin \theta)$ is the straight line anchored at $r = r_0$ and inclined at the angle ξ . The presented velocities and Lorentz factors were calculated in the locally non-rotating frame (see Eqs. (10)-(12)). As we can see from Eq. (8), the particles which are forced to move on rigidly rotating planar trajectories approach the speed of light at the light cylinder. This simply demonstrates that no physical solutions exists on and beyond light cylinders for purely poloidal magnetic field structures.

4.2. Force-free magnetosphere with non-zero azimuthal magnetic field component

Not necessarily such constraints apply for magnetosphere if taking into account presence of toroidal magnetic field component which is induced by poloidal electrical currents. In this case the Ferraro's law about iso-rotation still applies, i.e. magnetic field lines and, therefore, particle trajectories, still rotate rigidly, however, due to the presence of the toroidal magnetic component the rotating trajectories are not planar and the test particles may pass the light cylinder sliding on magnetic field lines in the opposite direction to the rotation of magnetic field surfaces, i.e. with $d\phi'/dt < 0$, which takes place if $\phi'_{,\theta} < 0$. This can be concluded from Eq. (8) after rewriting it in the form

$$u^t = \frac{\tilde{\epsilon}_0}{(-\tilde{g}_{tt})} \left(1 - \sqrt{\frac{1 - (-\tilde{g}_{tt})/\tilde{\epsilon}_0^2}{1 + (-\tilde{g}_{tt})\tilde{g}_{\theta\theta}/\tilde{g}_{t\theta}^2}} \right), \quad (19)$$

where the metric functions \tilde{g}_{ik} are calculated along trajectories $r = r(\theta; r_0)$ and $\phi' = \phi'(\theta; r_0)$. At the light cylinder both denominator and numerator ($-\tilde{g}_{tt}$ and the expression in brackets) become zero and applying the L'Hospital's rule one can check that u^t and, therefore, γ given by Eq. (10) is finite. Hence, the test particle can pass the light cylinder and proceed further provided

$$(\tilde{g}_{t\theta})^2 > \tilde{g}_{tt} \tilde{g}_{\theta\theta}, \quad (20)$$

i.e. for respectively large negative values of $\phi'_{,\theta}$,

$$(\phi'_{,\theta})^2 > \frac{\tilde{g}_{tt}(g_{\theta\theta} + g_{rr}(r_{,\theta})^2)}{(g_{t\phi} + g_{\phi\phi}\Omega_0)^2 - g_{\phi\phi}\tilde{g}_{tt}}. \quad (21)$$

Examples of kinematics of test particles for helical magnetic field structure are illustrated in Fig. 6. The velocity components and the Lorentz factor are computed for $r(\theta; r_0)$ given by Eq. (18) and for

$$\phi' = -\frac{\eta\Omega_0}{\cos\xi} (r \sin\theta - r_0). \quad (22)$$

The above choice of $\phi'(\theta; r_0)$ corresponds roughly with a poloidal magnetic field component scaling as $B_p \sim 1/(r \sin\theta)^2$ and toroidal component scaling as $B_\phi \sim 1/(r \sin\theta)$, while $\eta \approx -B_p/B_\phi|_{r \sin\theta=1/\Omega_0}$ (in Fig. 7 we plot a visualisation of such a shape of the magnetic field lines).

The upper panel of Fig. 6 presents the velocity and Lorentz factor profiles for a non-spinning BH. The particle is initially at rest with respect to the disk — its poloidal velocity component in the ZAMO frame is zero while its azimuthal velocity corresponds to the Keplerian angular velocity at r_0 . Once the particle leaves the equilibrium it starts to be centrifugally accelerated along the magnetic field line. The poloidal velocity component rapidly increases. Due to the fact that the magnetic field lines are inclined also in the azimuthal direction the particle starts to slide along them in the direction opposite to the disk rotation. Therefore, its angular velocity decreases below the initial value Ω_0 . The corresponding profile of the physical velocity in the azimuthal direction $v^{(\phi)}$ is shown. The light cylinder is crossed at $z \approx 14M$ with both velocity components close to $0.5c$. The profile of the Lorentz γ factor is shown with the solid line (please note the vertical scale for γ is marked on the right axis). Initially, it corresponds to

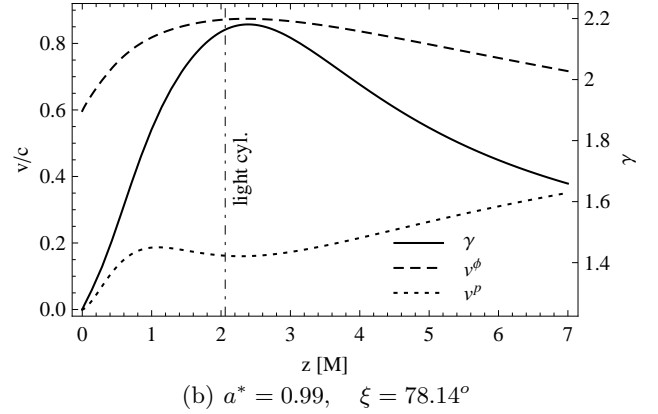
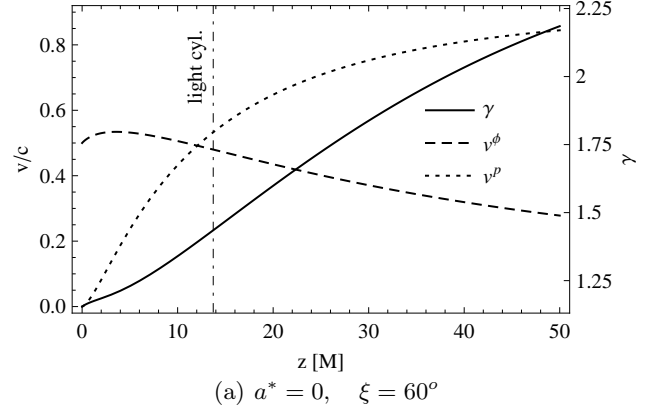


Fig. 6. The velocity components and the Lorentz factor γ of particles moving along magnetic field lines with non-zero azimuthal component anchored at r_{ms} and inclined at the critical angle $\xi = \xi_0$ for non-spinning (top) and spinning (bottom panel) BHs. Poloidal and azimuthal velocity components are marked by dotted and dashed lines, respectively. Solid curves present the Lorentz factor profiles.

the Keplerian angular velocity at r_{ms} (≈ 1.2 for $a^* = 0$ case). At the light cylinder $\gamma \approx 1.7$. The bottom panel of Fig. 6 presents a similar study of particle dynamics for a rotating BH case. Its behaviour is similar with exception to the fact that the γ factor is initially strongly dominated by the azimuthal velocity component.

We demonstrate in Fig. 8 the dependence of the test particle kinematics on ξ , r_0 and η . The upper panel shows that the lower the inclination angle ξ the more rapid is the particle acceleration. The middle panel presents the dependence on the η parameter which determines the magnetic field line torsion. The more 'twisted' is the line (corresponding to increasing η) the easier particle slides in the azimuthal direction and the resulting γ factor increases slower. Finally, the lower panel presents the dependence on the radius r_0 defining the location of the magnetic field line foot-point.

Obviously, illustrated in this section kinematics has only exemplary character and applies to the region in which the structure of the outflow is strongly dominated by the magneto-dynamics. For low mass loading rates, such a force-free approximation can be used to study the matter kinematics even far beyond the light cylinder. However, for high mass loading rates the force-free approximation can

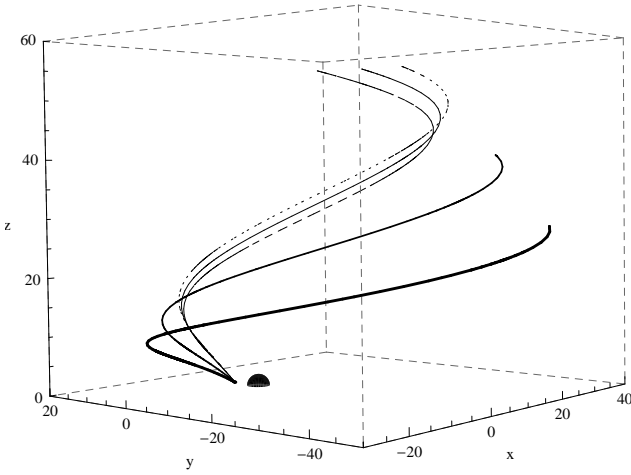


Fig. 7. Shape of the magnetic field lines with $\eta = 1.0$ for $\xi = 30^\circ$ (the thickest solid line), $\xi = 45^\circ$ and $\xi = 60^\circ$ (the thinnest solid line). For the latter ($\xi = 60^\circ$) two other curves are presented for $\eta = 0.95$ (dotted line) and $\eta = 1.05$ (dashed line). All lines are anchored at r_{ms} and the BH has zero spin. The black spot denotes location of the BH horizon.

break down even in the sub-Alfvénic region, deep within the light cylinder.

5. Discussion

Magnetocentrifugal scenario is applicable to the production of jets in ‘Newtonian’ objects like YSOs (Young Stellar Objects). However, it cannot explain the whole jet production process in BH accretion systems. This is because at least in idealized, steady, axisymmetric models with an accretion disk treated only as the boundary surface, efficient centrifugal mass loading makes the outflows too heavy to be accelerated up to the observed relativistic velocities. Favored mass loading scenarios for such objects involve pair production by photon-photon interactions. For typical BH accretion systems the coronal activities are enough powerful to support in the vicinity of the BH density of pairs by many orders of magnitude larger than the Goldreich-Julian density (Phinney 1983; McKinney 2005), which allows to treat the outflows in the ideal MHD approximation. By the same time, the rest mass-energy density of the pair plasma is by several orders lower than energy density of magnetic fields required to power luminous large scale jets in radio-loud objects, and this implies formation of relativistic, at least initially strongly Poynting flux dominated, outflows.

The e^+e^- jets can be powered by both rotating BHs (Blandford & Znajek 1977; Phinney 1983; Beskin 1997) and accretion disks (Blandford 1976; Lovelace 1976; Lovelace, Wang & Sulkanen 1987; Ustyugova et al. 2000). Such jets need external collimation to be effectively accelerated and converted to the matter dominated ones (Begelman & Li

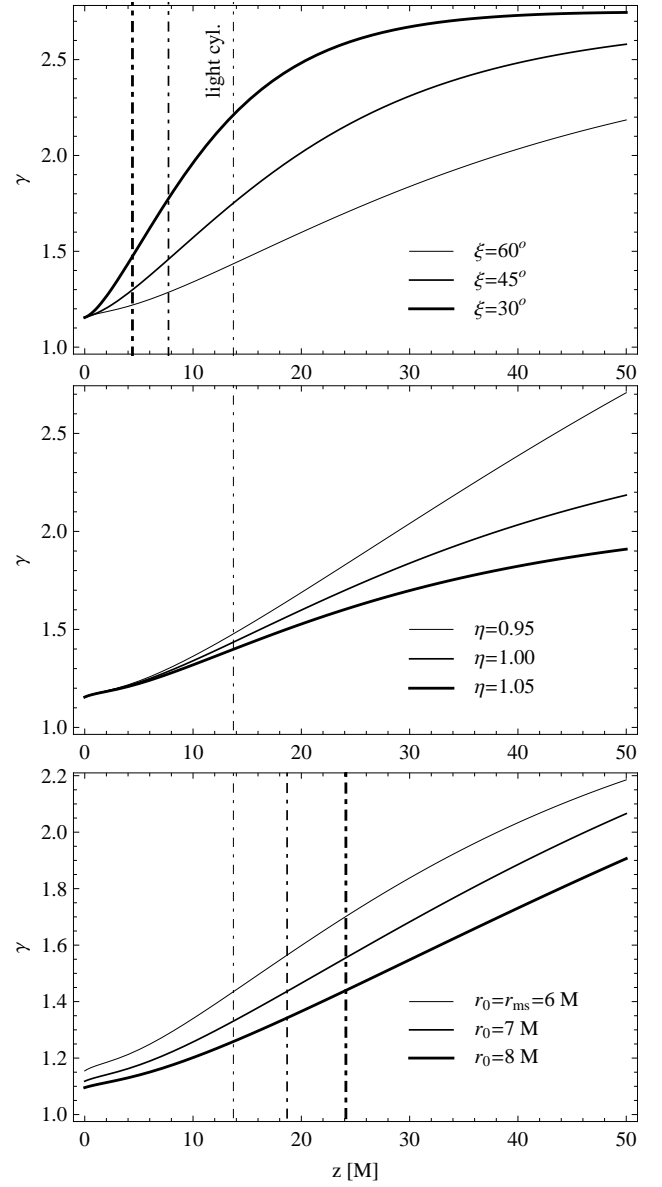


Fig. 8. The Lorentz γ factor dependence on the magnetic field line inclination angle ξ (top panel), η parameter (middle panel) and the r_0 radius (bottom panel) for a non-spinning BH. The vertical dashed lines denote crossing through the outer light cylinder. If not stated otherwise the parameters are: $\xi = 60^\circ$, $\eta = 1.0$ and $r = r_{ms}$.

1994; Narayan, McKinney, & Farmer 2007; Komissarov, et al. 2007; Lyubarsky 2009; Porth & Fendt 2010). The collimation is often considered to be provided by slower, barionic MHD outflows launched in the accretion disk (Sol, Pelletier, & Asseo 1989; Bogovalov & Tsinganos 2005; Gracia et al. 2005; Beskin & Nokhrina 2006). However, such a jet structure may need modification for jets launched around fast rotating BHs if the possibility of centrifugal launching of proton-electron outflows from innermost portions of accretion disk was taken into account. Since the inclination angle of the effective potential surfaces is maximal at the inner edge of a disk and rapidly drops with a radius (see Eq. 15 and Fig. 4, the p-e dominated outflow from the innermost portions of accretion disk is embraced by the Poynting flux dominated electron-positron outflow.

This implies less relativistic spines and more relativistic sheaths of jets produced by the accretion disk around fast rotating BHs, or a respective triple jet structure if taking into account the central contribution to the outflow from the BH magnetosphere.

The production of powerful jets by accretion disks, both centrifugally loaded and by pairs, requires strong large scale magnetic fields. Possibility of dragging of such fields by accreting plasma, originally suggested by Bisnovatyi-Kogan & Ruzmaikin (1974), is still debated (Lubow, Papaloizou, & Pringle 1994; Spruit & Uzdensky 2005; Bisnovatyi-Kogan & Lovelace 2007; Rothstein & Lovelace 2008; Beckwith, Hawley, & Krolik 2009). Related to the lack of the profound model of the evolution of magnetic fields in accretion disks, unknown remains radial distribution of inclination of magnetic field lines which is critical to establish a launching distance domain of centrifugal outflows and their initial collimation. And finally, even for a fixed large scale magnetic field intensity and geometry, mass loading rate and therefore the terminal speed of the centrifugal outflow depends very much on details of the vertical disk structure (Ogilvie & Livio 2001), which due to severe uncertainties is usually ignored. In particular, due to partial losses of angular momentum (taken away by the outflow) the boundary layers of the accretion disk likely become sub-Keplerian. As a result, proton-electron outflow may need some initial boost to pass the created potential barrier. It can be provided by heating or mechanically by some magnetic flaring activities and/or by radiation pressure of effectively super-Eddington flux. Existence of the additional potential barrier may significantly limit mass loading rate allowing proton-electron loaded outflows to reach at least mildly relativistic speeds. The resulting jet structure — mildly relativistic proton-electron component sandwiched between the pair dominated relativistic spine and sheath — albeit very speculative at the moment, is very promising from the observational point of view because may explain a significant proton content of AGN jets deduced from analyses of a matter content in blazars (Sikora & Madejski 2000; Ghisellini et al. 2009) and in radio lobes of powerful radio galaxies (Stawarz et al. 2007; Perlman et al. 2009).

6. Conclusions

Main results of this paper can be summarized as follows:

- An effective potential and light cylinders are investigated in the rigidly rotating frame in the Kerr metric. The intersection of equipotential surfaces with a geometrically thin disk at the annulus where a given angular velocity is equal to the Keplerian velocity gives the critical angle below which a cold outflow can be launched by centrifugal forces. The location of outer light cylinders is shown to depend strongly on radius and BH spin. For BH spin $a^* > 0.91$ and the Keplerian angular velocity at the marginally stable orbit the light-cylinder radius in the equatorial plane is enclosed within the ergosphere.
- The condition for magnetocentrifugal launching of jets obtained for Keplerian disks rotating around Kerr BHs by Cao (1997) and Lyutikov (2009) is confirmed. It tells us that the maximum inclination angle of magnetic flux surfaces at which cold matter can be extracted from the disk depends on a distance from the BH and on the BH spin. The condition shows that in case of very fast rotating BHs

the central outflows can be launched even along of almost vertically shaped magnetic surfaces.

- We show how kinematics of test particles pulled by centrifugal forces from a Keplerian disk can be algebraically determined for a given magnetic field structure in the force-free outflow approximation. Examples of test particle kinematics are illustrated and the condition for the toroidal magnetic field component is derived to allow the particle to cross the light cylinder.
- Possible implications for a jet structure are discussed as imposed by the condition for magnetocentrifugal launching of jets by inner portions of magnetized disks around fast rotating BHs. In this case a triple-component structure of a jet can be envisaged, with a proton-electron component of a jet being sandwiched between the relativistic pair dominated spine and sheath.

Acknowledgements. AS and MS acknowledge direct support by Polish Ph.D. NN203 304035 and MNiSW NN203 301635 grants, respectively.

References

- Bardeen, J.M., Press, W.H., & Teukolsky, S.A. 1972, *ApJ*, 178, 347
- Beckwith, K., Hawley, J., & Krolik, J.H. 2009, *arXiv:0906.2784*
- Begelman, M.C., & Li, Z.-Y. 1994, *ApJ*, 426, 269
- Beskin, V.S. 1997, *Soviet Physics Uspekhi*, 40, 659
- Beskin, V.S., & Nokhrina, E.E. 2006, *MNRAS*, 367, 375
- Bisnovatyi-Kogan, G.S., & Lovelace, R.V.E. 2007, *ApJ*, 667, L167
- Bisnovatyi-Kogan, G.S., & Ruzmaikin, A.A. 1974, *Ap&SS*, 28, 45
- Blandford, R.D. 1976, *MNRAS*, 176, 465
- Blandford, R.D. & Payne, D. G. 1982, *MNRAS*, 199, 883
- Blandford, R.D., & Znajek, R.L. 1977, *MNRAS*, 179, 433
- Bogovalov, S.V., & Tsinganos, K. 2005, *MNRAS*, 357, 918
- Cao, X. 1997, *MNRAS*, 291, 145
- Ferraro, V. C. A. 1937, *MNRAS*, 97, 458
- Ghisellini, G., Tavecchio, F., Foschini, L., Ghirlanda, G., Maraschi, L., & Celotti, A. 2009, *arXiv:0909.0932*
- Gracia, J., Tsinganos, K., & Bogovalov, S.V. 2005, *A&A*, 442, L7
- Komissarov, S.S., Barkov, M.V., Vlahakis, N., & Königl, A. 2007, *MNRAS*, 380, 51
- Lovelace, R.V.E. 1976, *Nat*, 262, 649
- Lovelace, R.V.E., Wang, J.C.L., & Sulkkanen, M.E. 1987, *ApJ*, 315, 504
- Lubow, S.H., Papaloizou, J.C.B., & Pringle, J.E. 1994, *MNRAS*, 267, 235
- Lyubarsky, Y.E. 2009, *MNRAS*, in press, *arXiv:0909.4819*
- Lyutikov, M. 2009, *MNRAS*, 396, 1545
- McKinney, J.C. 2005, *arXiv:astro-ph/0506368*
- Narayan, R., McKinney, J., & Farmer, A. 2007, *MNRAS*, 375, 548
- Ogilvie, G.I., & Livio, M. 2001, *ApJ*, 553, 158
- Perlman, E.S., Georganopoulos, M., May, E.M., & Kazanas, D. 2009, *arXiv:0910.3021*
- Phinney, E.S. 1983, PhD thesis, Cambridge University
- Porth, O., & Fendt, C. 2009, *arXiv:0911.3001*
- Rothstein, D.M., & Lovelace, R.V.E. 2008, *ApJ*, 677, 1221
- Sikora, M., & Madejski, G. 2000, *ApJ*, 534, 109
- Sol, H., Pelletier, G., & Asseo, E. 1989, *MNRAS*, 237, 411
- Spruit, H.C., & Uzdensky, D.A. 2005, *ApJ*, 629, 960
- Stawarz, L., Cheung, C.C., Harris, D.E., & Ostrowski, M. 2007, *ApJ*, 662, 213
- Ustyugova, G.V., Lovelace, R.V.E., Romanova, M.M., Li, H., & Colgate, S.A. 2000, *ApJ*, 541, L21